A Three Dimensional Analysis of Slotted Tube Resonator for MRI

Qiang Chen, Kunio Sawaya, Toru Uno, Saburo Adachi, Hisaaki Ochi, and Etsuji Yamamoto

Abstract— **A three dimensional model of a slotted tube resonator (STR) used as a probe in the magnetic resonance imaging (MRI), which is loaded by a dielectric body and surrounded by a conducting shield, is analyzed by using the variational method and the dyadic Green's function of a circular waveguide having a dielectric core. Three surface current modes are properly assumed to expand the currents on the STR. The characteristics such as the input impedance, the resonance frequency, the Q value, and the magnetic field distribution are obtained to show the effects of the dielectric body and the conducting shield. Some theoretical results are compared with the measured data to confirm the validity of the present analysis.**

I. Introduction

THE MRI (Magnetic Resonance Imaging) system, which can produce high-quality images in an arbitrary cross section of a human body, has been recognized as a new powerful technique for medical diagnosis and has gradually come to be employed recently in practical situations. In the MRI system, an RF probe is used to emit a uniform RF magnetic field over the human body and receive the magnetic resonance signal from the body for imaging.

Several kinds of RF probes have been developed. The bird-cage resonator (BCR) [1] is most commonly used for the MRI under high and low static magnetic field. The characteristics of the BCR including the effects of a lossy dielectric body and a conducting shield have been analyzed by using the moment method [2], [3]. The slotted tube resonator (STR) is also used especially for the MRI under low static field, which was proposed by Alderman and Grant [4]. Many efforts have been made to analyze the STR in order to show the properties of the probe and to design an optimum structure. In [5]–[8], the STR has been treated as a two dimensional model and numerical solutions have been obtained by using the finite element method. However, because the end rings and the lumped capacitors can not be included in these analyses, only the field distribution on a middle transverse plane has been calculated and the input impedance can not be obtained. On the other hand, another method called the electric equivalent circuit method [6], [9], can estimate the input impedance approximately but it can not show the field distribution and the effects of a dielectric body inserted into the STR. Recently, the moment method and the variational method have been applied by the present authors to analyze a three dimensional model of the STR [10], [11]. Numerical results of the current distribution, the electromagnetic field distribution and the input impedance have been obtained. These results have shown a high level of agreement with the measurement. However, the effects of the dielectric body have not been evaluated.

The purpose of this paper is to analyze the properties of three dimensional model of the STR loaded by a dielectric body and surrounded by a conducting shield by using the variational method. This method offers several advantages over the previous methods. Because of the stationary property of the variational expression of the input impedance, accurate impedance can be obtained. Since the three dimensional model is more rigorous than the previous two dimensional models, any components of the electromagnetic field can be calculated anywhere in the imaging region.

First, the variational expression for the input impedance of the STR is given. Then, the exact dyadic Green's function of a conducting circular waveguide including a lossy dielectric cylinder, and the expressions of the self and the mutual impedance between the basis functions, which are used to expand the unknown surface current on the probe conductor, are derived. Numerical results such as the input impedance, the resonance frequency, the field distribution, and the Q value are obtained to investigate the effects of the shield and the dielectric body. Some numerical results are compared with the experiment results to confirm the validity of the present method.

Although the quadrature operation (radiation and reception of circularly polarized field) [1] is used in the practical MRI, the single operation (linear polarization) is analyzed in this paper. However, the present numerical results such as the input impedance, the magnetic field distribution, and the percentage of loss can be used to deduce the properties of the quadrature operation, because there is no coupling between two driving points of the STR with the quadrature operation when the geometry of the body and the shield is axially symmetric. Furthermore, the analysis of the STR of the quadrature operation can be performed by extending the present method.

II. Formulation of the Problem

Fig. 1 shows the geometry of the model for the present analysis which involves the STR, a cylindrical conducting shield, and a cylindrical dielectric body. The STR is composed of six parts, i.e., two vertical strips called arms, two outer rings

Manuscript received July 28, 1993; revised February 4, 1994. The Associate Editor responsible for coordinating the review of this paper and recommending its publication was D. Nishimura.

Q. Chen, K. Sawaya, T. Uno, and S. Adachi are with the Department of Electrical Engineering, Faculty of Engineering, Tohoku University, Sendai 980, Japan; e-mail: chenq@sawaya.ecei.tohoku.ac.jp.

H. Ochi and E. Yamamoto are with the Central Research Laboratory, Hitachi Limited, Kokubunji 185, Japan.

IEEE Log Number 9403425.

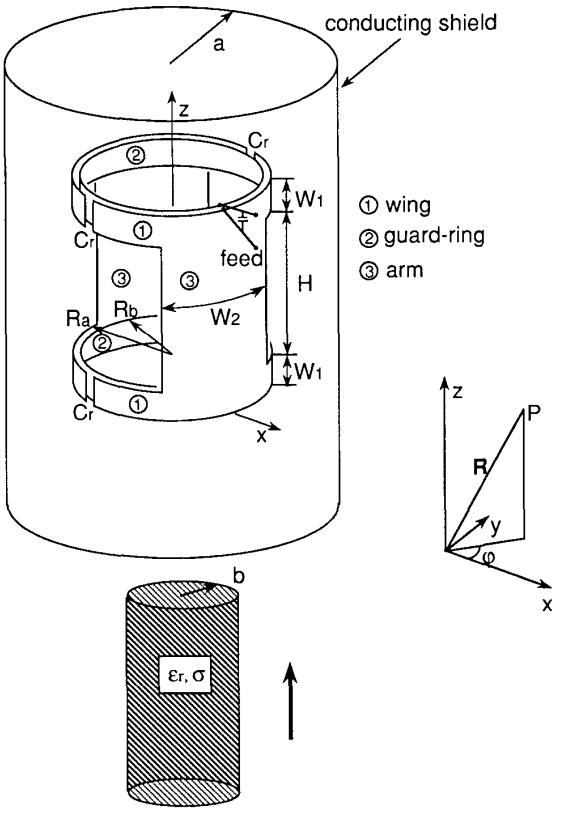

Fig. 1. Geometry of the slotted tube resonator loaded by a dielectric cylinder and surrounded by a conducting shield.

with radius R_a called wings, and two inner rings with radius R_b called guard-rings. Four chip capacitors C_r are attached to the wings for tuning the resonance frequency. Teflon sheets are inserted between the guard-rings and the wings. A capacitor C_m is connected parallel to the feed point for the sake of the impedance matching. The shield with radius a, the dielectric cylinder with radius b, and the STR are placed coaxially. Both the shield and the dielectric cylinder are assumed to be infinitely long for the simplicity of the analysis.

It is expected that the input impedance can be obtained with a high level of accuracy by using the variational method when a few number of properly selected basis functions are used to expand the unknown current. In our previous analysis of the unloaded STR [11], only three basis functions were used but the accuracy of the results was satisfactory. Therefore, we use the same basis functions to expand the surface current on the STR, i.e.,

$$\mathbf{I}(\mathbf{R}) = \sum_{k=1}^{3} \alpha_k \mathbf{f}_k(\mathbf{R}), \tag{1}$$

where α_k ($k = 1 \sim 3$) are unknown coefficients and $\mathbf{f}_k(\mathbf{R})$ is the basis functions given by

$$\begin{cases} |\mathbf{f}_1| = & 2, & \text{mode 1} \\ |\mathbf{f}_2| = & \cos 0.5\varphi, & \text{mode 2} \\ |\mathbf{f}_3| = & |\sin \varphi|. & \text{mode 3.} \end{cases} \tag{2}$$

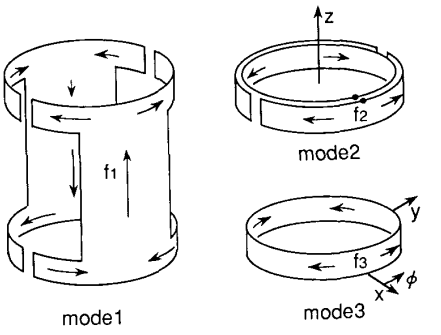

Fig. 2. Three expansion modes of surface current on the slotted tube resonator.

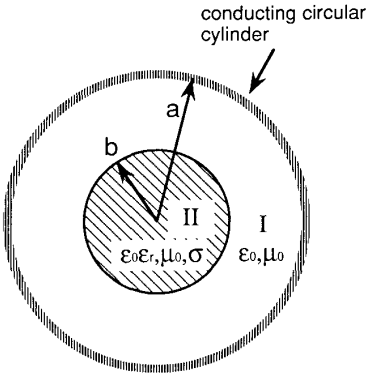

Fig. 3. Circularly cylindrical waveguide with a dielectric core.

The direction of each vector is indicated by arrows in Fig. 2. The surface current density is given by

$$\mathbf{J}(\mathbf{R}) = \mathbf{I}(\mathbf{R})/w(\mathbf{R}), \tag{3}$$

where $w(\mathbf{R})$ is the local width of the probe surface perpendicular to the direction of the current. The variational expression for the input impedance of the STR is expressed as,

$$Z_{\text{in}} = \frac{1}{4\alpha_2^2} \left\{ j\omega\mu \int_S \int_S \mathbf{J}(\mathbf{R}) \cdot \overline{\mathbf{G}}(\mathbf{R}, \mathbf{R}') \cdot \mathbf{J}(\mathbf{R}') dS' dS + \int_S \left[\left(\sum_{k=1}^{4} \delta(l - l_k) Z_c + Z_s \right) |\mathbf{J}(\mathbf{R})|^2 \right] dS \right\}, \tag{4}$$

where $\overline{\mathbf{G}}(\mathbf{R}, \mathbf{R}')$ denotes the dyadic Green's function of a circular cylindrical waveguide having a core of dielectric cylinder, and its expression is derived in Appendix A. The region of the integral denoted by S is the probe surface. Z_c is the impedance of the lumped capacitor C_r: $Z_c = 1/j\omega C_r$, and Z_s is the surface impedance of the copper [13]. l is the distance along the direction of the current and $\delta(x)$ is the Dirac delta function. $l = l_1, l_2, l_3$, and l_4 indicate the positions of the four lumped capacitors. In (4), the first integral is the reaction appearing in the ordinary variational expression of the antenna problem [14]. The second integral represents the electric power stored in the lumped capacitors and the loss power due to the copper loss of the probe conductor.

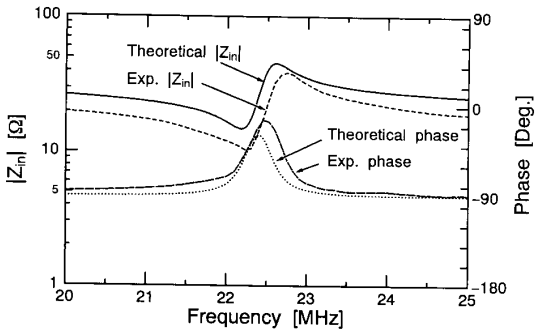

Fig. 4. Input impedance when the radius of the shield is 200 mm.

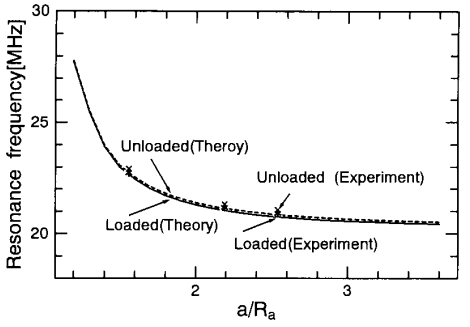

Fig. 5. Resonance frequency versus the radius of the shield.

According to the variational theory, the partial differentiation of Z_{in} with respect to each coefficient α_k should be zero. Assuming α_2 to be unity, the following equations can be obtained:

$$\begin{cases} \frac{\partial Z_{\text{in}}}{\partial \alpha_1} = 0, \\ \alpha_2 = 1, \\ \frac{\partial Z_{\text{in}}}{\partial \alpha_3} = 0. \end{cases} \tag{5}$$

By substituting (4) into (5), we get a simultaneous equation given by

$$\begin{cases} (Z_{11} + 4Z_c)\alpha_1 + Z_{12} + Z_{13}\alpha_3 = \sqrt{2}Z_c \\ Z_{13}\alpha_1 + Z_{23} + Z_{33}\alpha_3 = 0. \end{cases} \tag{6}$$

We can obtain the values of the unknown coefficients α_k ($k = 1, 3$) numerically. By substituting the current distribution into (4), we can calculate the input impedance as,

$$Z_{\text{in}} = \frac{1}{4}\left[\alpha_1 Z_{12} + Z_{22} + \alpha_3 Z_{23} + (1 - \sqrt{2}\alpha_1)Z_c\right], \tag{7}$$

where Z_{ij} denotes the self and the mutual impedance between the three modes defined by

$$Z_{ij} = j\omega\mu \int_S \int_S \mathbf{f}_i(\mathbf{R}) \cdot \overline{\mathbf{G}}(\mathbf{R}, \mathbf{R}') \cdot \mathbf{f}_j(\mathbf{R}') dS' dS + \int_S \frac{Z_s}{w^2(\mathbf{R})} |\mathbf{f}_i(\mathbf{R})| \cdot |\mathbf{f}_j(\mathbf{R})| dS. \tag{8}$$

Because the above expression includes a double surface integral over the surface of the STR, an infinite integral with respect to the wave number h and a infinite summation, the numerical computation of the Z_{ij} will cost too much CPU time. Therefore, we have evaluated the double surface integral in a closed form so that the Z_{ij} is expressed in a form containing only the single summation and the infinite integral. Since the analytical integration process is lengthy and the expressions of Z_{ij} are very complicated, only the expression of Z_{33} is given in appendix B. The complete expressions of self and mutual impedance are available in [16].

Once the surface current on the STR is obtained by solving (6), the electromagnetic field emitted by the STR can be evaluated by

$$\mathbf{E}(\mathbf{R}) = -j\omega\mu \int_S \overline{\mathbf{G}}(\mathbf{R}, \mathbf{R}') \cdot \mathbf{J}(\mathbf{R}')\, dS, \tag{9}$$

$$\mathbf{H}(\mathbf{R}) = \frac{j}{\omega\mu} \nabla \times \mathbf{E}(\mathbf{R}). \tag{10}$$

The electromagnetic field distribution are valid in the entire region inside the shield except for the close vicinity of the surface of the STR.

III. Numerical Results and Discussion

As a numerical example, the characteristics of the STR used in the imaging of a human head is calculated. The radii of the wing and the guard-ring are $R_a = 128$ mm and $R_b = 126$ mm, respectively. The height of the slots is $H = 230$ mm and the aperture angle is 93° which corresponds to the width of the arms $W_2 = 195$ mm. The width of both the wing and the guard-ring is $W_1 = 35$ mm. The capacitors C_r and C_m are 205 pF and 164 pF, respectively. The dielectric properties of the dielectric body with a radius of 97 mm have been chosen to approximate the equivalent human head. The electric constant is $\epsilon_r = 60$ and the conductivity is $\sigma = 0.3$ S/m. The copper loss of the STR, the dielectric losses of the tantalum capacitors C_r and C_m (Q factor $= 10^3$) are incorporated in the calculation, whereas the copper loss of the shielding cylinder is neglected. The effect of the Teflon sheets between the guard-rings and the wings is also neglected.

In order to show the validity of the analysis, the input impedance of the loaded STR inside the cylinder is measured. The STR is fabricated with copper strips having a thickness of about 0.5 mm. The configuration of the STR used in the experiment is the same as that of the theoretical model. Three circular copper cylinders are used in the experiment as the shielding cylinder. They are all about 1.5 m long and have radii of $a = 200$ mm, 280 mm and 325 mm, respectively. A 1.5 m long phantom with a radius of 97 mm, which is filled with NaCl solution, has been used as the dielectric body.

The input impedance of the STR is calculated and shown in Fig. 4, together with the measured data for the case of $a = 200$ mm. The agreement between the theory and the experiment is satisfactory.

Since the STR is used at the resonance frequency which has to be tuned to the spin frequency of the atomic nucleus to be imaged, it is important to know the shift of the resonance frequency that occurs when the radius of the cylinder is changed and the dielectric cylinder is loaded. The shift of the resonance frequency as a function of the radius of the cylinder is shown in Fig. 5, where the resonance frequency is obtained by searching for the frequency at which the imaginary part of

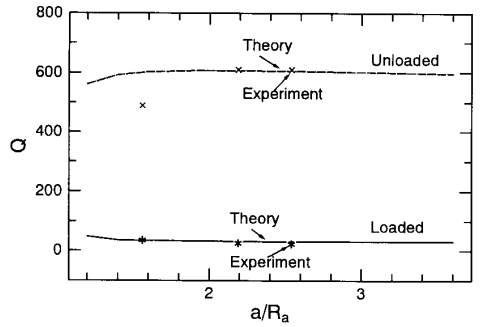

Fig. 6. Q factor versus the radius of the shield.

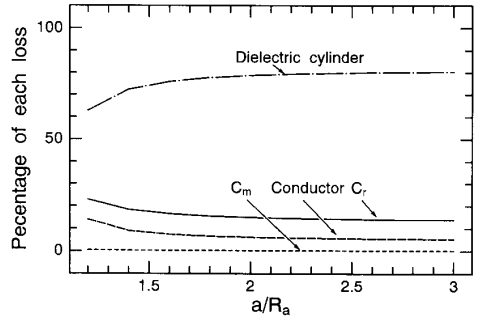

Fig. 7. Percentage of each loss versus the radius of the shield.

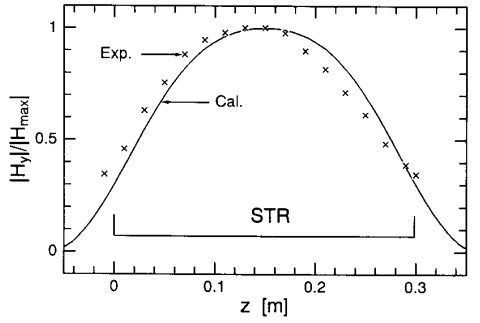

Fig. 8. Normalized magnetic field distribution along z-axis.

the input impedance becomes zero. A high level of agreement between the theory and the experiment is obtained to confirm the validity of the analysis. It is noted that the cylinder with the radius $a \leq 2R_a$ will increase the resonance frequency of the STR significantly while the dielectric cylinder does not affect the resonance frequency apparently.

The total loss can be estimated by the Q value, which is evaluated by $f_0/\Delta f$, where f_0 is the resonance frequency and Δf is the frequency width in which the magnitude of the input impedance satisfies the condition, $|Z_{\text{in}}(f)| \geq |Z_{\text{in}}(f_0)|/\sqrt{2}$. The theoretical and the experimental results of the Q value are plotted in Fig. 6. The theoretical results fairly agree with the measured data. When the radius of the shield decreases, the Q value without the body decreases whereas the Q value in the presence of the body increases.

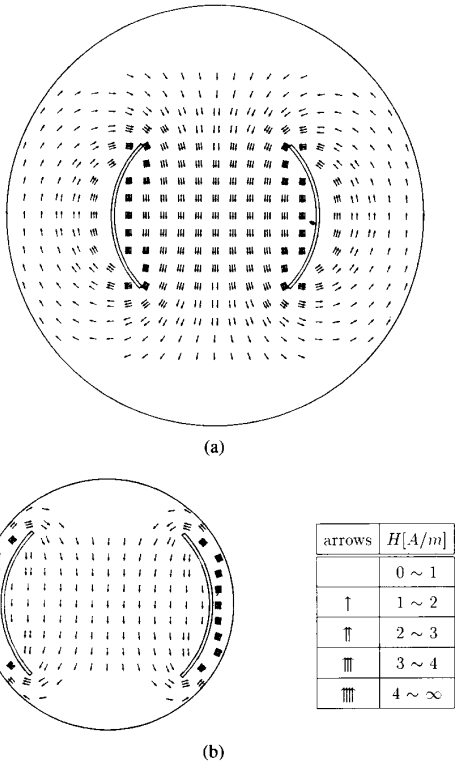

Fig. 9. Distribution of magnitude of the magnetic field on the middle cross-section for (a) $a/R_a = 2$ and (b) $a/R_a = 1.2$, when the input power is 1 watt.

The power loss of the model can be divided into the dielectric losses of the body and the capacitors, and the copper losses of the STR and the shield. In the present analysis, the copper loss of the shield is neglected. The percentage of each loss at the resonance frequency is also calculated and shown in Fig. 7, where the radius of the dielectric body is 85 mm. It is clear that the loss due to dielectric cylinder is dominant although its percentage decreases as the radius of the shield decreases. The second largest loss is that due to the loss of the capacitor C_r, and the copper loss and the loss due to the C_m are very small.

Fig. 8 shows the relative magnitude of component $|H_y|/|H_{y0}|$ along the z-axis at the resonance frequency (21.4 MHz) when the radius of the shield is 256 mm, i.e., twice of the radius of the probe, where H_{y0} is the value at the center of the probe ($x = y = 0$, $z = 150$ mm). The theoretical results and measured data obtained in the case of no dielectric body are plotted in the same figure for the comparison. Although the magnetic field distribution in the x-y plane has been published by using the two dimensional model [5]–[8], the magnetic field along the z-axis shown in Fig. 8 has so far not been reported, except for the measurement results [9].

Fig. 9 shows the mapping of magnitudes of the magnetic field distribution of the STR having the dielectric core in the cross section of $z = W_1 + H/2$ for the ratio of $a/R_a = 1.2$ and 2, where the input power is 1 watt. The arrow indicates the

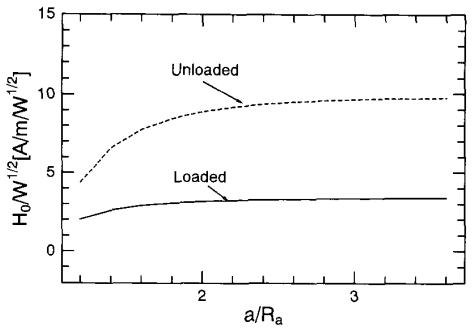

Fig. 10. Sensitivity of the slotted tube resonator versus the radius of the shield.

direction of the magnetic field. Since the variational expression of the input impedance has a stationary property, the input impedance can be obtained accurately. However, the boundary condition on the probe conductor is not satisfied completely and the field in the close vicinity of the conductor can not be obtained accurately. Therefore, the magnetic field in the close vicinity of the probe conductor is not shown in Fig. 9. The larger shielding cylinder brings little effects on the field distribution, and a uniform field distribution similar to that for the case of free space is observed [10]. While the smaller shielding cylinder tends to disturb the field and makes the magnitude weak in the imaging area significantly.

The sensitivity of the probes used for MRI can be defined by the ratio $H_0/\sqrt{P}$, where H_0 is the magnitude of the magnetic field at the center of the probe and P denotes the total input power in the probe. The sensitivity of the STR is shown in Fig. 10 as a function of the ratio a/R_a. The dielectric body decreases the sensitivity greatly because of the dielectric loss. It is also indicated that the ratio of a/R_a is required to be greater than approximately 2 in order to obtain the high sensitivity of the STR.

It is concluded from these field calculations (Figs. 8 and 10) that the strength of the magnetic field decreases greatly in the presence of the dielectric body. However, the relative magnetic field is almost the same to the case without the dielectric body.

IV. Conclusion

The slotted tube resonator (STR) surrounded by a conducting circular cylinder and loaded by a dielectric cylinder has been analyzed by using the variational method and the dyadic Green's function of a circular waveguide with a dielectric core. A method using three surface current modes has been proposed to expand the surface current on the STR. Although the probe has a complicated strip structure, the required CPU time was short and the accuracy of the results was satisfactory. The validity of present analysis has been confirmed by the experiment. Because of the presence of the cylindrical shield, the resonance frequency increases rapidly and the sensitivity of the STR decreases significantly when the ratio of a/R_a becomes less than approximately two. It has been shown that the effects of the dielectric cylinder on the resonance frequency and the relative magnitude distribution of the magnetic field are very small, but the dielectric body decreases the sensitivity greatly. Although only the single operation has been treated in this paper, the numerical results can be used to deduce the properties of the practical STR of the quadrature operation.

Appendix A

The expression of the dyadic Green's function of a cylindrical waveguide with a cylindrical dielectric core shown in Fig. 3 is derived in this Appendix. Based on the principle of superposition, the dyadic Green's function can be expressed as

$$\overline{\mathbf{G}} = \begin{cases} \overline{\mathbf{G}}_0 + \overline{\mathbf{G}}_s^{11}, & \text{in region I} \\ \overline{\mathbf{G}}_s^{21}, & \text{in region II,} \end{cases}$$

where $\overline{\mathbf{G}}_0(\mathbf{R},\mathbf{R}')$ is the Green's function for the ordinary cylindrical waveguide, $\overline{\mathbf{G}}_s^{(11)}(\mathbf{R},\mathbf{R}')$ and $\overline{\mathbf{G}}_s^{(21)}(\mathbf{R},\mathbf{R}')$ are scattering components. $\overline{\mathbf{G}}_0(\mathbf{R},\mathbf{R}')$ is expressed by [15]

$$\overline{\mathbf{G}}_0(\mathbf{R},\mathbf{R}') = -\frac{j}{8\pi}\sum_{n=0}^{\infty}\int_{-\infty}^{\infty} dh \frac{2-\delta}{\eta^2}\cdot \begin{cases} \mathbf{A}_{n\eta}(h)\mathbf{M}'_{n\eta}(-h) + \mathbf{B}_{n\eta}(h)\mathbf{N}'_{n\eta}(-h), & r \geq r' \\ \mathbf{M}_{n\eta}(h)\mathbf{A}'_{n\eta}(-h) + \mathbf{N}_{n\eta}(h)\mathbf{B}'_{n\eta}(-h), & r \leq r' \end{cases}$$

where η is defined by $\eta = \sqrt{k_0^2 - h^2}$ and $k_0 = \omega\sqrt{\mu_0\epsilon_0}$ is the wavenumber in free space. δ denotes the Kronecher delta function defined with respect to n as,

$$\delta = \begin{cases} 0, & n = 0 \\ 1, & n \neq 0 \end{cases} \tag{A-1}$$

and $\mathbf{M}_{n\eta}$, $\mathbf{N}_{n\eta}$ are the well-known cylindrical vector wave functions that satisfy the vector wave equations in the cylindrical coordinate [15], i.e.,

$$\begin{aligned} \mathbf{M}_{n\eta}(h) &= \nabla \times \left[J_n(\eta r) \begin{matrix}\cos\\ \sin\end{matrix} n\varphi e^{-jhz}\hat{\mathbf{z}}\right] \\ &= \left[\mp \frac{nJ_n(\eta r)}{r} \begin{matrix}\sin\\ \cos\end{matrix} n\varphi \hat{\mathbf{r}} - \frac{\partial J_n(\eta r)}{\partial r} \begin{matrix}\cos\\ \sin\end{matrix} n\varphi\hat{\varphi}\right] e^{-jhz}, \end{aligned} \tag{A-2}$$

$$\begin{aligned} \mathbf{N}_{n\eta}(h) &= \frac{1}{k_0}\nabla\times\nabla\times\left[J_n(\eta r)\begin{matrix}\cos\\ \sin\end{matrix} n\varphi\, e^{-jhz}\hat{\mathbf{z}}\right] \\ &= \frac{1}{k_0}\left[-jh\frac{\partial J_n(\eta r)}{\partial r}\begin{matrix}\cos\\ \sin\end{matrix} n\varphi\hat{\mathbf{r}} \right. \\ &\quad \pm \frac{jhn}{r} J_n(\eta r)\begin{matrix}\sin\\ \cos\end{matrix} n\varphi\hat{\varphi} \\ &\quad \left. + \eta^2 J_n(\eta r)\begin{matrix}\cos\\ \sin\end{matrix} n\varphi\hat{\mathbf{z}}\right] e^{-jhz}, \end{aligned} \tag{A-3}$$

where, $J_n(x)$ and $H_n^{(2)}(x)$ are the Bessel and the Hankel functions, respectively. They are defined by

$$J_n(x) = \sum_{k=0}^{\infty}\frac{(-1)^k}{k!(n+k)}\left(\frac{x}{2}\right)^{n+2k}, \tag{A-4}$$

$$H_n^{(2)}(x) = \lim_{\nu\to n}\frac{e^{-j\nu\pi}J_\nu(x) - J_{\nu-1}(x)}{-j\sin\nu\pi}, \tag{A-5}$$

and the derivative of the Bessel function can be obtained by

$$\frac{\partial J_n(x)}{\partial x} = \frac{nJ_n(x)}{x} - J_{n+1}(x). \tag{A-6}$$

In this paper, the Bessel and Hankel functions and their derivatives were performed by using the Bessel-Hankel function codes provided by the computer center of Tohoku University.

The vector coefficients $\mathbf{A}_{n\eta}$, $\mathbf{B}_{n\eta}$ are expressed as,

$$\mathbf{A}_{n\eta} = \mathbf{M}_{n\eta} - \left.\frac{\partial H_n^{(2)}(\eta r)/\partial r}{\partial J_n(\eta r)/\partial r}\right|_{r=a} \mathbf{N}_{n\eta}, \tag{A-7}$$

$$\mathbf{B}_{n\eta} = \mathbf{M}_{n\eta} - \frac{H_n^{(2)}(\eta a)}{J_n(\eta a)}\mathbf{N}_{n\eta}, \tag{A-8}$$

to satisfy boundary condition on the conducting surface of the shield ($r = a$).

The scattering components $\overline{\mathbf{G}}_s^{(11)}(\mathbf{R}, \mathbf{R}')$ and $\overline{\mathbf{G}}_s^{(21)}(\mathbf{R}, \mathbf{R}')$ should have the following forms:

$$\begin{aligned}\overline{\mathbf{G}}_s^{(11)}(\mathbf{R}, \mathbf{R}') = &-\frac{j}{8\pi}\sum_{n=0}^{\infty}\int_{-\infty}^{\infty} dh \frac{2-\delta}{\eta^2}\cdot \\ &\left[[a_n\mathbf{A}_{n\eta}(h) + b_n\mathbf{B}_{n\eta}(h)]\mathbf{A}'_{n\eta}(-h)\right. \\ &\left. + [c_n\mathbf{A}_{n\eta}(h) + d_n\mathbf{B}_{n\eta}(h)]\mathbf{B}'_{n\eta}(-h)\right],\end{aligned} \tag{A-9}$$

$$\begin{aligned}\overline{\mathbf{G}}_s^{(21)}(\mathbf{R}, \mathbf{R}') = &-\frac{j}{8\pi}\sum_{n=0}^{\infty}\int_{-\infty}^{\infty} dh \frac{2-\delta}{\eta^2}\cdot \\ &\left[[e_n\mathbf{M}_{n\xi}(h) + f_n\mathbf{N}_{n\xi}(h)]\mathbf{A}'_{n\eta}(-h)\right. \\ &\left. + [g_n\mathbf{M}_{n\xi}(h) + h_n\mathbf{N}_{n\xi}(h)]\mathbf{B}'_{n\eta}(-h)\right], \\ &r \le r'\end{aligned} \tag{A-10}$$

where $\xi = \sqrt{k^2 - h^2}$ and k is a complex wavenumber defined by $k = k_0\sqrt{1 - j\sigma/\omega\epsilon_0\epsilon_r}$. The dielectric constant and the conductivity of the dielectric cylinder are denoted by ϵ_r and σ, respectively.

The boundary conditions at the interface of $r = b$, i.e.,

$$\begin{cases} \hat{\mathbf{r}} \times \left(\mathbf{G}_0 + \mathbf{G}_s^{(11)}\right) = \hat{\mathbf{r}} \times \mathbf{G}_s^{(21)}, & r = b \\ \hat{\mathbf{r}} \times \nabla \times \left(\mathbf{G}_0 + \mathbf{G}_s^{(11)}\right) = \hat{\mathbf{r}} \times \nabla \times \mathbf{G}_s^{(21)}, & r = b \end{cases} \tag{A-11}$$

enable us to determine the unknown coefficients of a_n, b_n, c_n, d_n, e_n, f_n, g_n and h_n appearing in (A-9) and (A-10) by the following matrix equations:

$$[D_1] = [U]^{-1}[V_1], \tag{A-12}$$

and

$$[D_2] = [U]^{-1}[V_2], \tag{A-13}$$

where

$$[V_1] = \begin{bmatrix} \frac{\partial J_n(\eta b)}{\partial b} \\ 0 \\ \pm\frac{\chi}{\mu_1}J_n(\eta b) \\ -\frac{\eta^2}{\mu_1}J_n(\eta b) \end{bmatrix}, \quad [V_2] = \begin{bmatrix} \mp\frac{\chi}{k_1}J_n(\eta b) \\ \frac{-\eta^2}{k_1}J_n(\eta b) \\ \frac{k_1}{\mu_1}\frac{\partial J_n(\eta b)}{\partial b} \\ 0 \end{bmatrix},$$

$$[D_1] = \begin{bmatrix} a_{e^n}^o \\ b_{o^n}^e \\ e_{e^n}^o \\ f_{e^n}^o \end{bmatrix}, \quad [D_2] = \begin{bmatrix} c_{e^n}^o \\ d_{o^n}^e \\ g_{e^n}^o \\ h_{o^n}^e \end{bmatrix},$$

$$[U] = \begin{bmatrix} -\dot{\Pi}'(\eta b) & \pm\frac{\chi}{k_1}\Pi(\eta b) & \frac{\partial J_n(\xi b)}{\partial b} & \mp\frac{\chi}{k_2}J_n(\xi b) \\ 0 & \frac{\eta^2}{k_1}\Pi(\eta b) & 0 & -\frac{\xi^2}{k_2}J_n(\xi b) \\ \mp\frac{\chi}{\mu_1}\Pi(\eta b) & -\frac{k_1}{\mu_1}\dot{\Pi}'(\eta b) & \pm\frac{\chi}{\mu_2}J_n(\xi b) & \frac{k_2}{\mu_2}\frac{\partial J_n(\xi b)}{\partial b} \\ \frac{\eta^2}{\mu_1}\Pi(\eta b) & 0 & -\frac{\xi^2}{\mu_2}J_n(\xi b) & 0 \end{bmatrix}, \tag{A-14}$$

$$\chi = \frac{jhn}{b}, \tag{A-15}$$

and Π, $\dot{\Pi}$, Π' and $\dot{\Pi}'$ are defined by

$$\Pi(\eta b) = \frac{J_n(\eta a)H_n^{(2)}(\eta b) - H_n^{(2)}(\eta a)J_n(\eta b)}{J_n(\eta a)} \tag{A-16}$$

$$\dot{\Pi}(\eta b) = \frac{J'_n(\eta a)H_n^{(2)}(\eta b) - H_n^{(2)'}(\eta a)J_n(\eta b)}{J'_n(\eta a)} \tag{A-17}$$

$$\Pi'(\eta b) = \frac{J_n(\eta a)H_n^{(2)'}(\eta b) - H_n^{(2)}(\eta a)J'_n(\eta b)}{J_n(\eta a)} \tag{A-18}$$

$$\dot{\Pi}'(\eta b) = \frac{J'_n(\eta a)H_n^{(2)'}(\eta b) - H_n^{(2)'}(\eta a)J'_n(\eta b)}{J'_n(\eta a)} \tag{A-19}$$

respectively. The radius of the shield and dielectric cylinder are denoted by a and b, respectively. The prime of the Bessel and the Hankel functions are defined by

$$J'_n(\eta a) = \left.\frac{\partial J_n(\eta x)}{\partial x}\right|_{x=a}, \qquad H_n^{(2)'}(\eta a) = \left.\frac{\partial H_n^{(2)}(\eta x)}{\partial x}\right|_{x=a}. \tag{A-20}$$

APPENDIX B

In this Appendix, the expression of the Z_{33} is shown as an example. Since the mode 3 has a distribution of $|\sin\varphi|$, as (8), Z_{33} can be derived as,

$$\begin{aligned} Z_{33} &= j\omega\mu\int_S\int_S |\sin\varphi|\hat{\varphi}\cdot\overline{\mathbf{G}}(\mathbf{R}, \mathbf{R}')\cdot\hat{\varphi}|\sin\varphi'|dS'dS \\ &\quad + \int_S \frac{Z_s}{W_1^2}\sin^2\varphi dS \\ &= 4j\omega\mu R_b^2\int_0^{W_1}dz\int_0^{\pi}d\varphi\int_0^{W_1}dz'\int_0^{\pi'}d\varphi' \\ &\quad \times \sin\varphi\bar{\mathbf{G}}_{\varphi\varphi}(\mathbf{R}, \mathbf{R}')\sin\varphi' + \frac{2Z_sR_b}{W_1}\int_0^{\pi}\sin^2\varphi d\varphi \\ &= \frac{\omega\mu R_b^2}{2\pi W_1^2}\sum_{n=0}^{\infty}\int_{-\infty}^{\infty}dh\frac{2-\delta_0}{\eta^2} \\ &\quad \times \left[(a_o\dot{\Pi}'(\eta R_b) + J'_n(\eta R_b))\dot{\Pi}'(\eta R_b)\right. \\ &\quad - \left(\frac{b_e\Pi(\eta R_b)\dot{\Pi}'(\eta R_b)}{R_b} - \frac{c_o\dot{\Pi}'(\eta R_b)\Pi(\eta R_b)}{R_b}\right)\frac{jhn}{k_1} \\ &\quad \left. + (d_e\Pi(\eta R_b) + J_n(\eta R_b))\Pi(\eta R_b)\frac{h^2n^2}{k_1^2R_b^2}\right]I_p(h)I_p(-h) \\ &\quad + \frac{Z_sR_b\pi}{W_1} \end{aligned} \tag{B-1}$$

where,

$$I_p(h) = \int_0^{W_1} dz \int_0^{\pi} \sin n\varphi \sin \varphi e^{-jhz} d\varphi = \begin{cases} -\frac{\pi}{2jh}(e^{-jhW_1} - 1) & (n = 1) \\ 0 & (n \neq 1). \end{cases} \quad \text{(B-2)}$$

REFERENCES

[1] V. J. Sank, C. N. Chen, and D. I. Hoult, "A quadrature coil for the adult human head," *J. Magn. Reson.*, vol. 69, pp. 236–242, 1986.

[2] H. Ochi, E. Yamamoto, K. Sawaya, and S. Adachi, "Analysis of MRI antenna inside an RF shield," *Trans. IEICE*, vol. J76-B-II, no. 2, pp. 79–85, Feb. 1993 (in Japanese).

[3] ——, "Analysis of MRI antenna loaded by a man model," *Trans. IEICE*, vol. J76-B-II, no. 4, pp. 253–259, Apr. 1993 (in Japanese).

[4] D. W. Alderman and D. M. Grant, "An efficient decoupler coil design which reduces heating in conductive samples in superconducting spectrometers," *J. Magn. Reson.*, vol. 34, pp. 425–433, 1979.

[5] L. W. Anne, L. Darrasse, J. Taquin, and M. Sauzade, "The slotted cylinder: An efficient probe for NMR imaging," *Magn. Reson. Med.*, vol. 2, pp. 20–28, 1985.

[6] D. H. Hong, S. W. Lee, J. W. Ra, and Z. H. Cho, "Whole body slotted tube resonator for proton NMR imaging at 2.0 Tesla," *Magn. Reson. Imag.*, vol. 5 no. 3, pp. 239–243, 1987.

[7] G. J. Kost, S. E. Anderson, G. B. Matson, and C. B. Conboy, "A cylindrical-window NMR probe with extended tuning range for studies of the developing heart," *J. Magn. Reson.*, vol. 82, no. 1, pp. 238–252, Mar. 1989.

[8] T. K. Foo, C. E. Hayes, and Y. W. Kang, "An analytical model for the design of RF resonators for MR body imaging," *Magn. Reson. Med.*, vol. 21, pp. 165–177, 1991.

[9] E. J. Nijhof, "Slotted resonator: Principles and applications for high-frequency imaging and spectroscopy on electrically conducting sample," *Magn. Reson. Imag.*, vol. 8, no. 3, pp. 345–349, 1990.

[10] Q. Chen, K. Sawaya, S. Adachi, H. Ochi, and E. Yamamoto, "Analysis of slotted tube resonator for MRI," *Trans. IEICE*, vol. J75-B-II, no. 8, pp. 602–605, Aug. 1992 (in Japanese).

[11] ——, "Analysis of MRI slotted tube resonator having a shield of conducting circular cylinder," *IEICE Trans. Commun.*, vol. E76-B, no. 5, pp. 553–560, May 1993.

[12] C. E. Haves, W. A. Edelstein, J. F. Schenck, O. M. Mueller, and M. Eash, "An efficient, highly homogeneous radiofrequency coil for whole-bodly NMR imaging at 1.5 T," *J. Magn. Reson.*, vol. 63, no. 3, pp. 622–628, July 1985.

[13] D. M. Pozar, *Microwave Engineering*. Reading, MA: Addison-Wesley, 1990, p. 44.

[14] R. E. Collin and F. J. Zucker, *Antenna Theory, Part I*. New York: McGraw-Hill, 1969, p. 53.

[15] C. T. Tai, *Dyadic Green's Functions in Electromagnetic Theory*. Intext Educational Publishers, 1971.

[16] Q. Chen, "Study on magnetic resonance imaging antennas," Ph.D. dissertation, Faculty of Engineering, Tohoku University, Japan, 1994.